PAPER

Check for updates

An immunosensor for the detection of *N*-(carboxymethyl)lysine - a diabetic biomarker†

Priyanga Kumar,[ab] Noel Nesakumar,[c] Srinivasan Vedantham[cd] and John Bosco Balaguru Rayappan [iD] *[ab]

Carboxymethyl-lysine (CML) is a well-known lysine product that strongly correlates with type 2 diabetes mellitus (T2DM), and its elevated levels are significantly associated with renal impairment and T2DM-related complications. Thus, it is imperative to quantify CML levels and recognize the onset of hyperglycemia and its consequences. In this context, the development of an electrochemical immunosensor for the rapid and ultralow-level detection of CML was attempted. The fabrication of the working electrode involves the covalent immobilization of anti-CML/EDC-NHS on the surface of a carbon quantum dot (CQD)-modified glassy carbon electrode (GCE). The immunosensor exhibited two discrete linear concentration ranges of 0.5–5.0 ng mL^{-1} and 5.5–10.0 ng mL^{-1}, with limits of detection and quantification of 0.027 and 0.087 ng mL^{-1} and 0.16 and 0.51 ng mL^{-1}, respectively. The observed specificity and other merits of the sensor make it suitable for testing human plasma samples.

1. Introduction

Diabetes mellitus (DM) is a metabolic disorder characterized by elevated blood sugar levels caused by deficient insulin production and reduced insulin sensitivity.[1] Abnormal regulation of glucose metabolism leads to long-term complications. It is a global contributor to morbidity and mortality and a significant health concern in most developed countries.[2] Diabetes affects an estimated 422 million individuals worldwide, most of whom reside in low- and middle-income nations. This disorder is directly responsible for 1.5 million deaths per year.[3] In this context, researchers have started focusing on identifying potential diabetes biomarkers, such as glucose,[4] HbA1c,[5] fructose,[6] methylglyoxal,[7] glycated albumin,[8] and islet-cell cytoplasmic AAb.[9] Although many biomarkers are available for diabetes detection, CML has a significant impact on diet-controlled diabetes compared to T2DM. CML is one of the advanced glycation end-products (AGEs) that acts as an active component of hazardous metabolites in diabetes mellitus. CML is produced due to the thermal treatment of foods, oxidation of fructose-lysine in the glycolytic pathway, as well as the interaction of

lysine with lipid peroxidation and amino acids in the advanced lipid peroxidation end-product (ALE) pathway.[10] CML is the initial glycoxidation product formed from the interaction between glucose and lysine under physiological conditions.[11] CML has also been found in significant concentrations in thermally treated meals containing milk byproducts and ascorbate.[12] CML is a well-defined AGE precursor in long-lived proteins and has been used as a biomarker for oxidative stress in biological systems.[13] In middle-aged and free-living individuals, elevated fasting levels of the circulating AGE CML, indicate the onset of diabetes.[14] This has led researchers to focus on the presence of CML in food.[15] Elevated blood glucose levels stimulate protein glycation, leading to the development of CML. Once formed, CML tends to accumulate in different tissues over time. Complications include diabetic retinopathy, diabetic nephropathy, and cardiovascular disorders. In addition, the development of AGEs is common in the context of oxidative stress and CML. The measurement of CML can offer valuable insights into a patient's oxidative stress level, as diabetes is associated with increased oxidative stress.

It is widely recognised that high glucose levels may contribute to the development of CML and increase the risk of several pathological conditions, including diabetes and cardiovascular diseases.[16] Therefore, elevated glucose levels may result from oxidative stress or metabolic dysregulation, which can increase glycation and lead to the accumulation of CML and its associated complications.[17] Multiple studies have shown that CML levels are significantly higher in patients with diabetes and related complications than in healthy individuals.[18] In this context, Hull *et al.* studied the levels of CML in food items such as coffee, dairy products, fish, and cereal-

[a]Centre for Nanotechnology & Advanced Biomaterials (CeNTAB), SASTRA Deemed University, Thanjavur, Tamil Nadu, 613 401, India. E-mail: rjbosco@ece.sastra.edu; Fax: +91 4362 264 120; Tel: +91 4362 350009. ext. 2255

[b]School of Electrical & Electronics Engineering (SEEE), SASTRA Deemed University, Thanjavur, 613 401, India

[c]School of Chemical & Biotechnology (SCBT), SASTRA Deemed University, Thanjavur, 613 401, India

[d]DifGen Pharmaceuticals Private Ltd Hyderabad, India

† Electronic supplementary information (ESI) available. See DOI: https://doi.org/10.1039/d5ra00968e

derived products, and surprisingly reported 514.4 mg per 100 g of protein in dairy products.[19] The CML concentrations in these food items are expected to increase by up to 200-fold with higher cooking temperature. The incorporation of protein and fat into bread products can promote CML formation. Moreover, CML levels in bakery products typically increase when ingredients rich in fat, sugar, and protein are added to the formulations.[20] Jara et al. examined CML levels in serum samples from patients with diabetes, including those with T2DM and T1DM. Each participant completed a 24-hour dietary recall test specifically designed to measure CML intake, in addition to a food frequency questionnaire. This study confirmed that the consumption of dry and high-temperature cooked foods, such as milk powder and fried meat, increased CML levels in blood serum, particularly in patients with diabetes.[21]

The levels of CML vary in the different media of the human metabolic system. The normal levels of CML are 1.2 μmol mol^{-1} lysine in blood plasma,[22] 1.79 mg dL^{-1} in urine excretion samples,[23] 5.5 ng mg^{-1} protein in serum samples,[23] and 0.2 nmol mg^{-1} protein[23] in tissue samples. The various pathways for the production of CML indicate that the formation of CML is enhanced by a complex interaction of oxidative processes involving reactive carbonyls, lipids, and carbohydrates. CML is recognized as a byproduct of glycoxidation and lipid oxidation and functions as an indicator of oxidative stress and lipid per-oxidation. The CML produced through various pathways exhibits distinct levels depending on the medium of production.[24]

Several attempts have been made in the past decade for the effective detection of glucose to predict and analyze diabetes levels for regular monitoring.[25–27] In addition, several reports have described other biomarkers, such as methylglyoxal,[28] glycated albumin,[29] HbA1C,[30] and anti-glutamic acid.[31] Although many sensors have been developed for the detection of various diabetes biomarkers, all of those sensors were intended for the diagnosis of T1DM. With this background, a plethora of researchers started working on detecting AGE products related to T2DM using polyclonal antibodies,[32] HPLC,[33] immunohistochemistry,[34] or ELISA[35] based on their distinct fluorescence properties. The development of sensor devices has been stimulated by the increased number of possibilities for quick diagnostic analysis. In this regard, this study focused on detecting the T2DM biomarker CML, which has a strong correlation with a healthy lifestyle. Considering this background, the development of a label-free electrochemical immunosensor is essential for selecting a better sensing method for CML detection. In addition, it is ideal to compare the current response of anti-CML-modified GCE with and without CML using a redox mediator via immunocomplex. Immunosensors have garnered significant attention owing to their inherent advantages, including cost-effectiveness, sensitivity, and seamless integration with downsizing methodologies.[36] In the case of an immunosensor, the signal from the antibody–antigen interaction creates an analytical response in an electrochemical immunosensor.[37] There are three possible ways to immobilize the captured antibody via covalent binding, physical adsorption, or electrostatic trapping onto the nano-material surface-modified electrode.[38] To overcome the growing demand for the early and ultrasensitive detection of analytes/

antigens, highly conductive materials are preferred as nano-interfaces.[39] Carbon-based nanomaterials gained more attention due to their many desirable characteristics, including high stability, excellent electrocatalytic activity, large surface area, superior conductivity,[40] fluorescent properties, and biocompatibility. CQDs are extensively employed as substrates to facilitate efficient bioreceptor immobilization and expedite electron transfer to the electrode surface.[41] The interaction between CQDs and anti-CML is facilitated through the utilization of an amide cross-linker. EDC, a compound consisting of 1-ethyl-3-(3-dimethylaminopropyl) carbodiimide, is used to activate the functional group in CQDs by forming an intermediate ester. Subsequently, N-hydroxysuccinimide (NHS) was used to change the reactive intermediates from unstable to stable esters.[42] In this study, an electrochemical-based immunosensor was developed to detect the levels of CML with the aid of anti-CML via immunocomplex formation. Carbon-based materials like CQDs were utilized as the nanointerface to initiate the electron transport rate using electrochemical techniques such as cyclic voltammetry (CV), differential potential voltammetry (DPV), and amperometry analysis.

2. Materials and methodology

2.1. Synthesis of CQDs

500 g of citrus orange peels were obtained from the local market and washed and cleaned with deionized water. The sliced peels were dried under sunlight for 15 days and then dried in a hot air oven for 1 h at 60 °C. The dried pieces were ground to obtain an orange peel powder. An equimolar ratio of orange peel powder to urea (1 : 1) was allowed to dissolve in 150 mL of deionized water under stirring at 800 rpm for 8 h. The precipitate mixture was exposed to a hydrothermal process at 180 °C for 6 h.[43] To remove any solid particles, the hydrothermally treated solution was subjected to dialysis using an 8 kDa membrane. The filtered mixture was then collected and stored at 4 °C (Scheme 1).
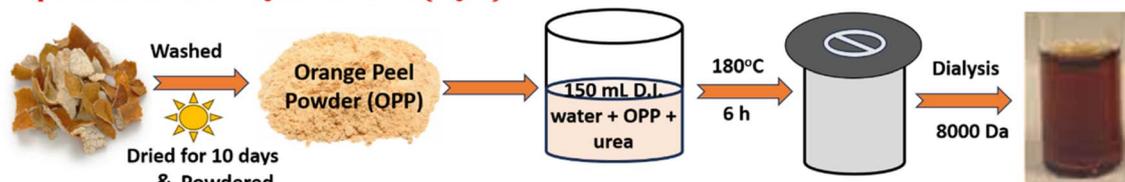
2.2. Fabrication of the working electrode and electrochemical characterization

The surface area of the GCE was modified with the as-prepared CQDs using the drop-casting method and dried at 28 °C. In addition, 0.005 M EDC and NHS were combined in an equimolar proportion (1 : 1) by constantly swirling the blend in NaCl at 600 rpm for 30 min. The obtained mixture was then combined with 5 μL of anti-CML at room temperature and agitated for 4 h. Subsequently, a volume of 3 μL of the mixture was drop casted onto the surface of the GCE/CQDs. The carboxylic terminal groups of CQDs react with the anti-CML amine groups via the EDC/NHS cross-linker to form durable amide bonds. The unreacted loosely bound anti-CML was washed away using NaCl, and the fabricated GCE/CQDs/anti-CML/EDC-NHS was stored at 4 °C.
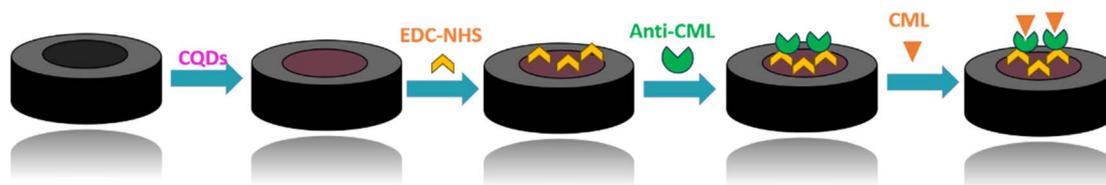
The electrochemical performance of the surface-modified GCE was examined using CV with 0.005 M of K$_3$[Fe(CN)$_6$] and 0.1 M NaCl at a pH of 7.0 at room temperature (301 K). The conventional three-electrode system was adapted to study the

Scheme 1 Schematic of the proposed work.

sensor performance of the surface-modified working electrode with the aid of the antigen–antibody interaction to determine the redox potential of the developed immunosensor. To improve the effectiveness of the interaction between the CQDs and CML, the CQD/anti-CML surface-modified electrode was incubated with CML for 300 s to attain a stable amide bond. The DPV and amperometric responses were analyzed with varying concentrations of CML.
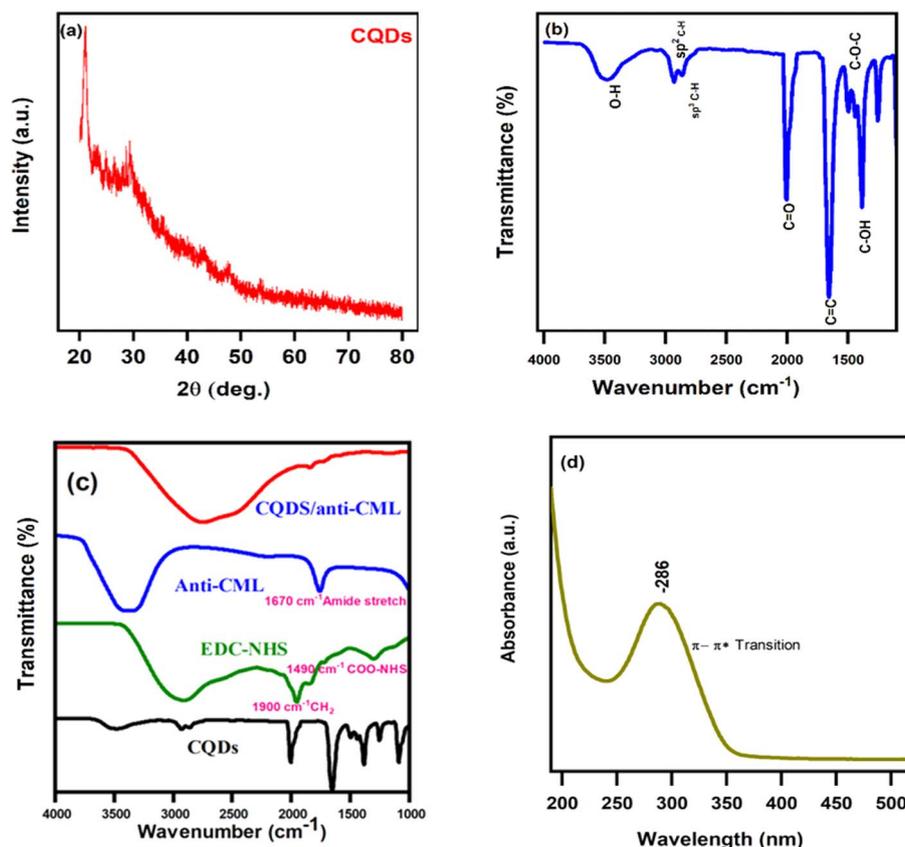

Fig. 1 (a) XRD patterns of the as-prepared CQDs, (b) Fourier transform infrared (FT-IR) spectrum of CQDs, (c) FT-IR spectra of the CQDs, EDC-NHS, anti-CML, and CQDs/EDC-NHS/CQDs-anti-CML, and (d) UV-vis spectrum of CQDs.

3. Results and discussion

3.1. Structural, functional, and optical analysis

The structural properties of the as-prepared CQDs were examined using an X-ray diffractometer (XRD) in the range of 20–80°, as shown in Fig. 1(a). The peak with an interlayer distance of 2.5 nm, observed at 22.7°, corresponds to the (002) plane formed due to the disordered stacking of CQDs. The peak at 27.5° is associated with the (100) plane of aromatic segment interlayer stacking in CQDs. In addition, the amorphous nature of the material confirms the formation of C-dots and is in good agreement with the literature.[44]

Fig. 1(b) shows the FT-IR spectrum of the as-prepared CQDs. The O–H stretching vibrations of the CQDs can be attributed to the wide band around 3490 cm^{-1}. The observed band at 2934 cm^{-1} corresponds to an sp^2 hybrid C–H stretching vibration, and the peak at 2866 cm^{-1} corresponds to an sp^3 hybrid C–H stretching vibration.[45] The sp^2 and sp^3 hybridizations were attributed to the citric nature of the orange peel powder. The peak at 2000 cm^{-1} indicates stretching at the C=O interface. The broadband detected at 1475 cm^{-1} is ascribed to the symmetrical stretching vibrations of C–O–C, whereas the band recorded at 1405 cm^{-1} corresponds to the asymmetric stretching vibrations of C–O–C from CQDs. Substantial hydrogen bonding causes the broadness. Fig. 1(c) shows the bond formation at 1670 cm^{-1} due to the amide bond between the amine group from EDC-NHS and anti-CML. The surface modification of the antigen–antibody on the surface of the CQDs was clarified from the FTIR spectra. The carbon dots exhibited an optical absorption peak in the ultraviolet (UV) region, specifically at 286 nm, with a tail that extended into the visible spectrum, as shown in Fig. 1(d). The aromatic sp^2 hybridization of the CQDs is attributed to the π–π* transition of the conjugated C=C band.[46]

3.2. Optimization of the surface-modified electrode

The impact of pH on the chemical reduction of CML was examined across a pH range extending from 4.0 to 11.0, as shown in Fig. 2(a). It was observed that pH 7 exhibited the most significant peak current response. The electrode kinetics of the bare GCE, GCE/CQDs, and GCE/CQDs/anti-CML electrodes were examined in the presence of 0.5 ng mL^{-1} of CML over a scan rate of 10–100 mVs^{-1}. A noticeable peak current was observed at a lower scan rate, along with a linear correlation with the scan rate in the observed current response. The electrochemical performance of the GCE/CQDs/anti-CML was characterized by a diffusion-controlled mechanism, exhibiting a linear regression of $R^2 = 0.98$ (Fig. S1†). The experimental parameters were tuned to optimize the immunosensor. The impact of various
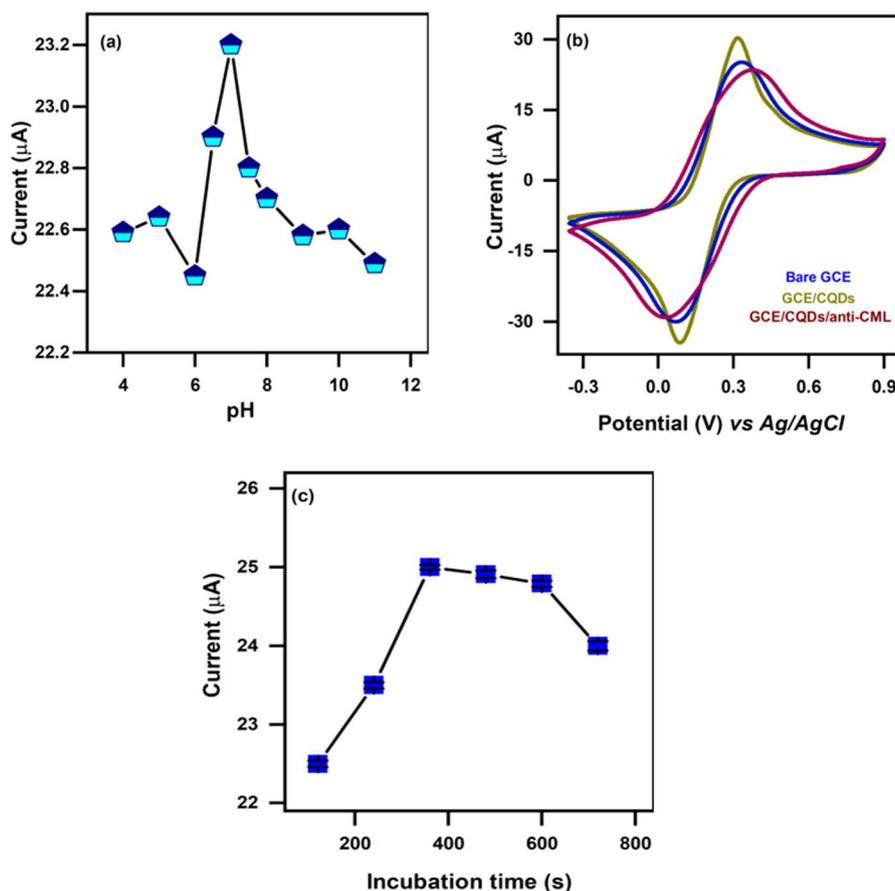

Fig. 2 (a) Influence of pH on antigen–antibody interaction of CML, (b) cyclic voltammograms of bare GCE, GCE/CQDs, and GCE/CQDs/anti-CML/NHS-EDC in the presence of 0.5 ng mL^{-1} of CML, and (c) influence of incubation time on the interaction of the antigen–antibody complex.

antibody–antigen incubation times on the efficacy of the immunosensor was investigated by regulating the quantity of antigen captured by the antibody (Fig. 2(b)).

The immunosensor performance was evaluated in the presence of 0.5 ng mL^{-1} of CML for various incubation durations, ranging from 2 to 12 min, as shown in Fig. 2(c). Upon increasing the incubation time, the inhibition rate increased after 6 min, and the post-inhibition proportion approached saturation. An immunocomplex formed when the antigen molecules captured the immobilized antibody molecules on the reformed electrode surface, indicating neutralization.

3.3. Electrochemical behavior of modified GC electrode

Control studies were conducted using various unmodified and modified GCE/CQD electrodes. To study the electrochemical behavior of the bare electrode, an unmodified GCE was subjected to CV analysis, and the minimal peak current was recorded in the presence of CML due to the redox properties of ferricyanide and NaCl. Furthermore, the surface of the bare GCE was modified with 3 μL of CQDs, and its current response was recorded, as shown in Fig. 2(b). The anti-CML-EDC/NHS coating was modified onto the surface of the GCE, and the current response was observed. As the concentration of CML increased, the current decreased. However, the efficacy of GCE/CQDs/anti-CML in

response to CML was reduced upon exposure to CML at a concentration of 0.5 ng mL^{-1} during incubation, due to the CML/anti-CML complex formation, which impedes the charge transfer properties. The implication of the step-by-step variation of the electrode *via* immunocomplex formation can be evaluated by the ratio of the electroactive surface area (ESA). The ESA values of the bare, CQD, and CQDs/anti-CML/EDC-NHS modified GCEs were estimated through the Randles–Sevcik equation and found to be 0.0403, 0.0517 and 0.0335 cm^2, respectively. The electron transfer rate of the CQDs/anti-CML modified electrode was 1.574×10^{-4} s^{-1}, and the surface coverage associated through binding was 7.27×10^{-11} M cm^{-2}.

3.4. DPV analysis

The DPV current response of GCE/CQDs/anti-CML was observed within the applied potential window of 0 to 0.8 V (*vs.* Ag/AgCl) in the presence of different concentrations of CML with an electrolyte containing a mixture of 0.005 M Fe (CN)6$^{3-/4-}$ and 0.1 M NaCl, as shown in Fig. 3(a). As the molar concentration of CML increased, the current response progressively decreased due to the formation of the immunological complex, which hindered the probe's ability to transfer charge. The developed biosensor exhibits two distinct linear concentration ranges: 0.5–5 ng mL^{-1} and 5–10 ng mL^{-1}, as shown in Fig. 3(b and c). The
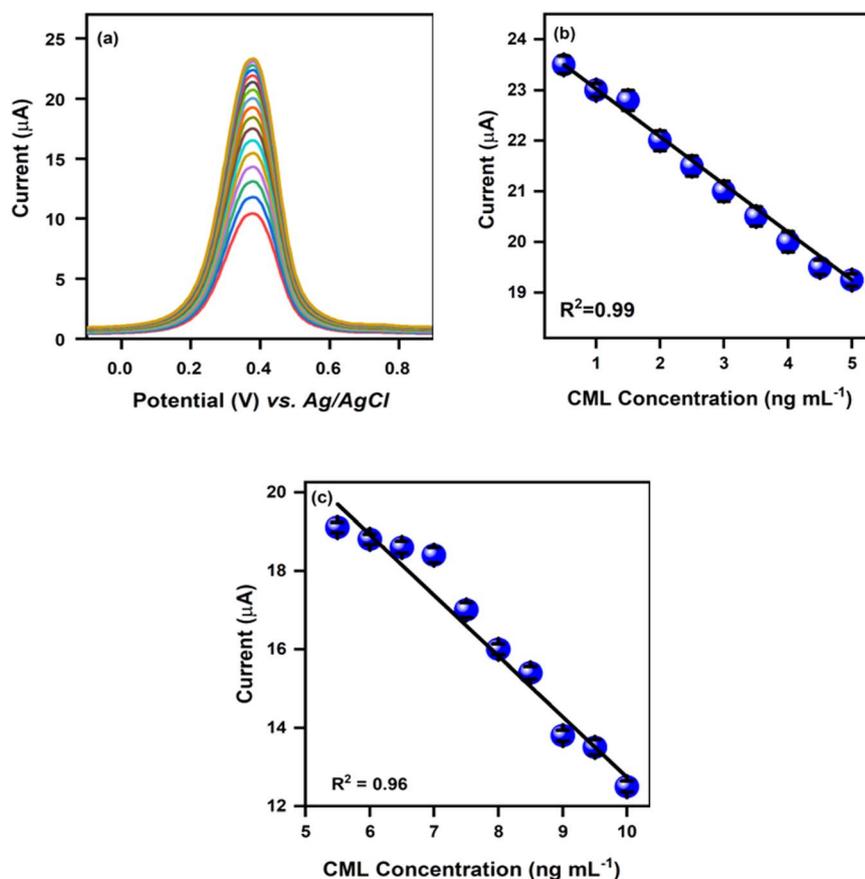

Fig. 3 (a) DPV of the CQDs/anti-CML/EDC-NHS modified GC electrodes in the presence of CML, (b) linear calibration curve for increasing CML concentrations of 0.5–5.0, and (c) 5.5–10.0 ng mL^{-1} with adjusted regression coefficients of $R^2 = 0.99$ and 0.96, respectively.

corresponding linear regression equations were $y = -0.94x + 23.9$ ($R^2 = 0.99$) and $y = -1.5x + 28.2$ ($R^2 = 0.96$), respectively. The limits of detection for the two ranges were 0.027 and 0.16 ng mL^{-1}, with corresponding limits of quantification of 0.087 and 0.51 ng mL^{-1}, respectively, calculated using the following formula:

$$\text{LOD} = \frac{3 \times \text{standard deviation of the response}}{\text{slope of the calibration curve}} \quad (1)$$

$$\text{LOQ} = 3.33 \times \text{LOD} \quad (2)$$

Fig. 4(a) shows the calibration curve for the voltammetric current response for increasing concentrations of the substrate (0.5–12 ng mL^{-1}). From the figure, it can be observed that there are two distinct linear ranges with different sensitivities, which are evident from their corresponding linear regression equations, whereas the concentration increased from 10–12 ng mL^{-1}, confirming the saturation state. The variation in sensitivity across the two linear ranges was due to the occupancy of the substrate at the active sites of the enzyme, as evidenced by the fractional saturation curve (Fig. 4(b$_1$)). As shown in Fig. 4(b$_2$), when the concentration of the substrate added to the 0.1 M KCl solution was 0 ng mL^{-1}, the fractional saturation was zero, indicating that there was no occupancy of the active sites of the antibody by the substrate. However, when the substrate concentration was increased from 0 to 5 ng mL^{-1}, a greater number of binding active sites were occupied by the substrate, increasing the fractional saturation to up to 42%. These results also suggested that nearly 42% of the active sites were occupied by the substrate. In contrast, upon further increasing the substrate concentration from 5 ng mL^{-1} to 10 ng mL^{-1}, the fractional saturation reached almost 73%, indicating that nearly 73% of the active sites had been occupied by the substrate. Because fractional saturation was in the range of 42–73% when the substrate concentration increased from 5 ng mL^{-1} to 10 ng mL^{-1}, fewer active sites were available in the antibody sites for the substrate to bind. This decreased the reaction rate, which in turn reduced the current intensity. Due to the decrease in current intensity, the sensitivity value determined across the

linear range of 5–10 ng mL^{-1} was also different from the sensitivity determined in the previous linear range (0.5–5 ng mL^{-1}). At the same time, the sensing mechanism remained unchanged. However, due to the change in fractional saturation and the limited availability of active sites, two different linear ranges with distinct sensitivities exist.

3.5. Impedance analysis

To evaluate the analytical abilities of the developed immunosensor, electrochemical impedance spectroscopy (EIS) was employed to determine various concentrations of CML. The variation in charge transfer resistance (R_{ct}) during surface-level modification is graphically represented using a Nyquist plot comprising a semi-circle and a linear segment, as shown in Fig. 5. The incorporation of the CQDs/anti-CML composite onto the bare GCE resulted in a reduction in the arc diameter of the CQDs and CML on the GCE, owing to the enhanced conductivity of the CQDs. The effective formation of covalent bonding between the CML antibody and the CQDs *via* EDC/NHS was demonstrated by the Nyquist plot; the R_{ct} value increased after adding anti-CML to the composite surface. The covalent binding of CML/anti-CML reduced the conductivity of the immunoelectrode, which impeded electron transfer. In the preceding stage of modification, when conjugated with CML or anti-CML, the impedance spectra exhibited an increase in R_{ct} on the Nyquist plot. The effective binding of the antigen and antibody by CML further hindered the transmission of electrons to the immunosensor interface. The EIS measurements confirmed the successful construction of the immunosensor.

3.6. Amperometry studies

To evaluate the developed sensor's selectivity and specificity against CML, amperometric analysis was performed at a voltage of 0.3 V between the GCE/CQDs/anti-CML-modified working electrode and the reference electrode. The effects of various CML concentrations on the amperometric current response were measured from 0.5 to 10 ng mL^{-1}. The constant current response exhibited a significant decrease with an increase in the levels of
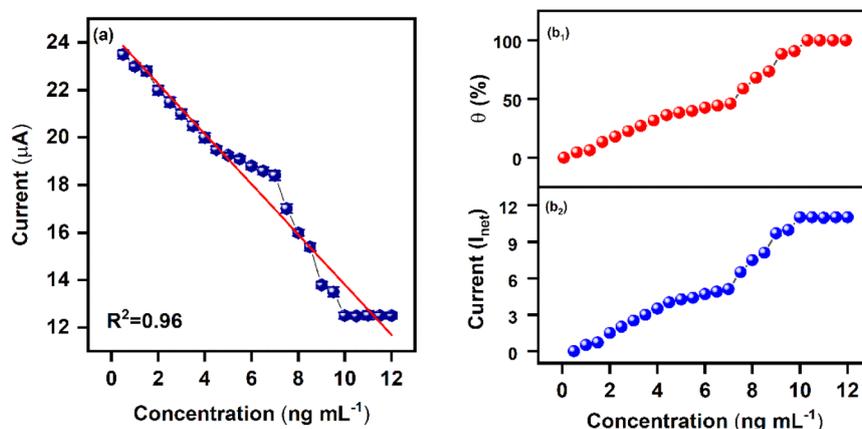

Fig. 4 (a) Linear calibration plot for increasing concentrations of CML, (b$_1$) fractional saturation (q), and (b$_2$) change in current (I_{net}) for increasing concentrations.

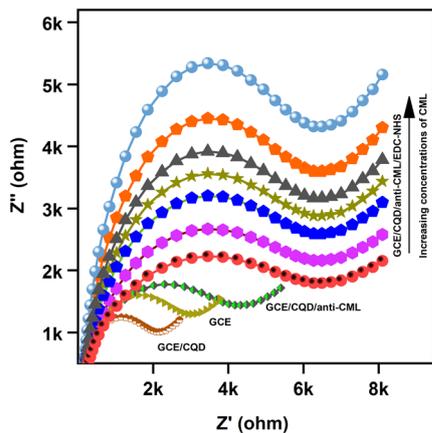© 2025 The Author(s). Published by the Royal Society of Chemistry

Fig. 5 Impedance spectra of the developed immunosensor for detecting various concentrations of CML.

CML. In response to CML, the linear calibration plots of the various concentration arrays displayed a linear trend ($y = -0.6x + 18.5$), as shown in Fig. 6(a). The developed biosensor's response time was anticipated to be less than 15 s. The biosensor exhibited an LOD of 0.09 ng mL^{-1} and a LOQ of 0.30 ng mL^{-1}, as shown in Fig. 6(b). The obtained results indicate that the developed immunosensor is capable of detecting ultralow levels of CML. In addition, the sensor reached a saturation level and exhibited a consistent current response at 0.5 ng mL^{-1} following anti-CML, suggesting the presence of an immunocomplex on GCE/CQDs/anti-CML.

3.7. Influence of potential interferants

The specificity of the developed immunosensor was also evaluated for the widely observed potential biomarkers in human blood plasma samples. The selectivity of the GCE/CQDs/anti-CML electrode was subjected to different interfering elements,

such as glucose, glutamic acid, fructose, ascorbic acid, glutathione, uric acid, methylglyoxal and paracetamol, with 0.5 ng mL^{-1} of CML. In the presence of interfering biomarkers, there was no substantial variation in the current response, which confirmed that the proposed sensor can overcome potential interfering biomarkers with a 10-fold surplus in concentration. With an overall variation in the current responses of less than 8%, the developed sensor appears to have a high degree of selectivity toward CML, as shown in Fig. 7.

3.8. Stability, repeatability and reproducibility

To examine the storage stability of the developed immunosensor, the variation in the current toward CML detection was assessed as a function of time. The peak current response was subsequently investigated for thirty days (Fig. 8(a)). The current response of the developed sensor exhibited a decline of 5.2% by
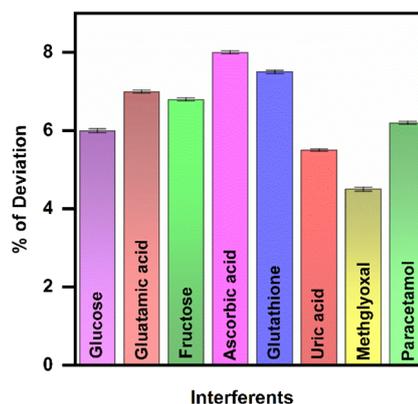

Fig. 7 Bar graph representation of current response deviation for various interfering species on CML.
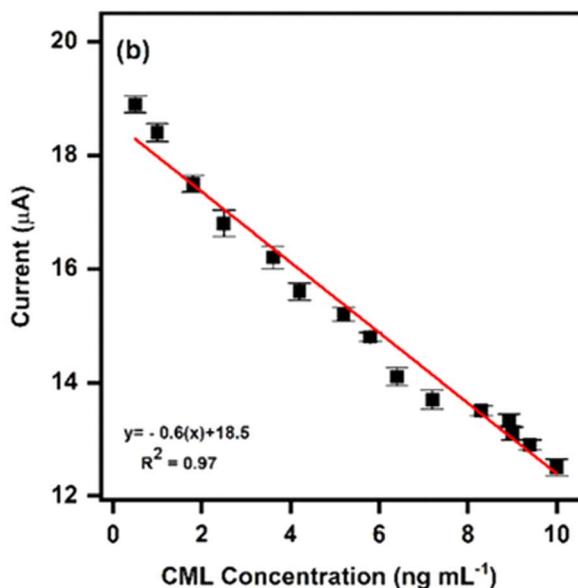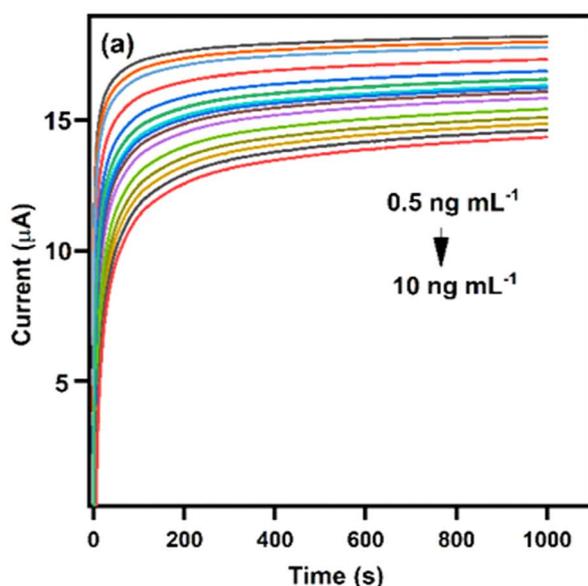

Fig. 6 (a) Amperometric current responses of the GCE/CQDs/anti-CML electrode at different CML concentrations; (b) calibration plot.
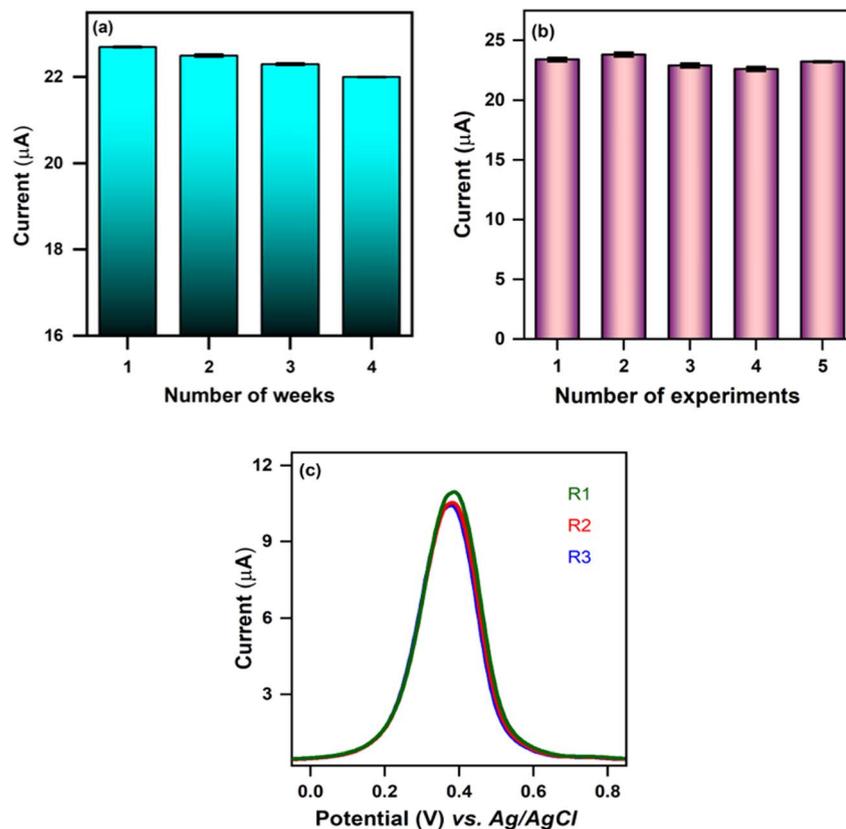
Fig. 8 DPV current responses of GCE/CQDs/anti-CML/NHS-EDC for (a) stability over four consecutive weeks, (b) repeatability across four different experiments, and (c) reproducibility using three different electrodes in the presence of CML.

Table 1 Comparative study of detection of CML[a]

Technique	Detection range	LOD	LOQ	Ref.
UPLC/MS	20–3500 ng mL^{-1}	1.3 ng mL^{-1}	4.1 ng mL^{-1}	47
LC/MS	10–1000 ng mL^{-1}	N/A	10 ng mL^{-1}	48
GC/MS	0.5–25 μmol	0.1 μmol mL^{-1}	0.20 pmol	49
IDMS	0.25–10 μM	N/A	0.16 μM	22
Electrochemical	0.5–2500 μg mL^{-1}	166 ng mL^{-1}	N/A	50
Electrochemical	0.5–10 ng mL^{-1}	0.027 ng mL^{-1}	0.087 ng mL^{-1}	Present work

[a] UPLC/MS–ultra-high performance liquid chromatography/mass spectroscopy; LC/MS–liquid chromatography/mass spectroscopy; GC/MS–gas chromatography/mass spectroscopy; IDMS–isotope dilution mass spectrometry.

the end of the month. The repeatability of the developed sensor was established by conducting five consecutive trials in the presence of 0.5 ng mL^{-1} of CML, and the corresponding current responses are shown in Fig. 8(b). The RSD was calculated to be 3.03%. To evaluate the reproducibility of the proposed sensor, electrode fabrication and CQD preparation were repeated several times. The current response for each modification was observed and plotted against the potential and is shown in Fig. 8(c). The developed sensor exhibited an RSD value of 0.05%. These outcomes indicated that the developed immunosensor exhibits stability and selectivity towards the detection of CML in real-time samples.

With this background, a recovery study was conducted using ringer lactate (RL) solution, and the recovery was found to be

96–102.5%. This method is thus more practical for real-time applications, and the developed sensor is appropriate for the detection of CML. Table 1 presents the comparison between the CML sensors reported in the literature and the current work. From this comparison, one can observe the ultra-low level detection capability of the current CML sensor.

4. Conclusion

In conclusion, electrochemical immunosensor capable of detecting the diabetic biomarker, CML, has been developed. The anti-CML immobilization process was significantly improved by the inclusion of the CQD-modified GCE interface. The reaction obtained from the probe species gradually

decreased as the binding between CML and anti-CML increased, thereby verifying the development of an efficient immunocomplex. The developed GCE/CQDs/anti-CML biosensor was used to quantitatively analyze CML. The developed electrochemical immunosensor exhibits sensitivity and stability throughout a wide range of values, as well as a low limit of detection. Additionally, a study was conducted to assess the recovery of CML in RL solution. A defined concentration of CML was introduced into the RL solution, and the recovery range was determined to be 94.6–102.5%. This confirms that the developed sensor is suitable for practical applications. The advanced electrochemical immunosensor can be employed to assess healthcare applications related to diabetes.

Data availability

Data will be made available on request.

Author contributions

Priyanga Kumar: investigation, data curation and writing original draft. Noel Nesakumar: formal analysis, interpretation and editing. Srinivasan Vedantham: formal analysis, validation, writing and editing. John Bosco Balaguru Rayappan: conceptualization, supervision, funding acquisition and editing.

Conflicts of interest

The authors declare no conflict of interest.

Acknowledgements

References

1 American Diabetes Association, *Diabetes Care*, 2009, **32**(suppl. 1), S62–S67.
2 E.-H. Yoo and S.-Y. Lee, *Sensors*, 2010, **10**, 4558–4576.
3 International Diabetes Federation, *IDF Diabetes Atlas*, International Diabetes Federation, Brussels, 10th edn, 2021.
4 A. J. Krentz and M. Hompesch, *Biomarkers Med.*, 2016, **10**, 1153–1166.
5 T. J. Lyons and A. Basu, *Transl. Res.*, 2012, **159**, 303–312.
6 Y. Chen, H. Lin, L. Qin, Y. Lu, L. Zhao, M. Xia, J. Jiang, X. Li, C. Yu, G. Zong, Y. Zheng, X. Gao, Q. Su and X. Li, *Diabetes Care*, 2020, **43**, 2217–2225.
7 L. Ramachandra Bhat, S. Vedantham, U. M. Krishnan and J. B. B. Rayappan, *Biosens. Bioelectron.*, 2019, **133**, 107–124.
8 P. A. C. Freitas, L. R. Ehlert and J. L. Camargo, *Arch Endocrinol. Metab.*, 2017, **61**, 296–304.
9 B. Dorcely, K. Katz, R. Jagannathan, S. S. Chiang, B. Oluwadare, I. J. Goldberg and M. Bergman, *Diabetes Metab. Syndr. Obes.*, 2017, **10**, 345–361.
10 Z.-Q. Wang, H.-P. Yao and Z. Sun, *World J. Diabetes*, 2023, **14**, 222–233.
11 K. A Ahmed, S. Muniandy and I. S. Ismail, *J. Clin. Biochem. Nutr.*, 2007, **41**, 97–105.
12 L. Li, Y. Zhuang, X. Zou, M. Chen, B. Cui, Y. Jiao and Y. Cheng, *Foods*, 2023, **12**(11), DOI: 10.3390/foods12112103.
13 H.-Y. Park, M.-J. Oh, Y. Park and Y. Kim, *Food Sci. Biotechnol.*, 2020, **29**, 487–491.
14 V. C. Luft, B. B. Duncan, M. I. Schmidt, L. E. Chambless, J. S. Pankow, R. C. Hoogeveen, D. J. Couper and G. Heiss, *Diabet Med.*, 2016, **33**, 1392–1398.
15 S. H. Assar, C. Moloney, M. Lima, R. Magee and J. M. Ames, *Amino Acids*, 2009, **36**, 317–326.
16 L. Ding, Y. Hou, J. Liu, X. Wang, Z. Wang, W. Ding and K. Zhao, *J. Renal Nutr.*, 2024, **34**, 154–160.
17 L. de Bari, A. Scirè, C. Minnelli, L. Cianfruglia, M. P. Kalapos and T. Armeni, *Antioxidants*, 2021, **10**, 1–17.
18 E. Lambrinou, T. B. Hansen and J. W. J. Beulens, *Eur J Prev Cardiol.*, 2019, **26**, 55–63.
19 G. Hull, J. Woodside, J. Ames and G. Cuskelly, *Food Chem.*, 2012, **131**, 170–174.
20 H. Boz, *J. Food Sci.*, 2023, **88**, 901–908.
21 N. Jara, M. J. Leal, D. Bunout, S. Hirsch, G. Barrera, L. Leiva and M. P. de la Maza, *Nutr. Hosp.*, 2012, **27**, 1272–1278.
22 N. J. Rankin, K. Burgess, S. Weidt, G. Wannamethee, N. Sattar and P. Welsh, *Ann. Clin. Biochem.*, 2019, **56**, 397–407.
23 Z. Wagner, I. Wittmann, I. Mazak, R. Schinzel, A. Heidland, R. Kientsch-Engel and J. Nagy, *Am. J. Kidney Dis.*, 2001, **38**, 785–791.
24 M. D. Eggen and M. A. Glomb, *J. Agric. Food Chem.*, 2021, **69**, 7960–7968.
25 S. H. Nguyen, P. K. T. Vu, H. M. Nguyen and M. T. Tran, *Sensors*, 2023, **23**(5), DOI: 10.3390/s23052841.
26 J. Wu, Y. Liu, H. Yin and M. Guo, *Am. J. Transl. Res.*, 2023, **15**, 3825–3837.
27 T. Saha, R. Del Caño, K. Mahato, E. De la Paz, C. Chen, S. Ding, L. Yin and J. Wang, *Chem. Rev.*, 2023, **123**, 7854–7889.
28 P. Kumar, N. Nesakumar, J. Gopal, S. Vedantham and J. B. B. Rayappan, *IEEE Sens. J.*, 2022, **22**, 15683–15690.
29 Z. Li, J. Zhang, G. Dai, F. Luo, Z. Chu, X. Geng, P. He, F. Zhang and Q. Wang, *J. Mater. Chem. B*, 2021, **9**, 9324–9332.
30 M. Thiruppathi, J.-F. Lee, C. C. Chen and J. A. Ho, *Sens. Actuators, B*, 2021, **329**, 129119.
31 X. Ma, C. Fang, J. Yan, Q. Zhao and Y. Tu, *Talanta*, 2018, **186**, 206–214.
32 G. S. Chadha and M. E. Morris, *Curr. Pharmacol. Rep.*, 2016, **2**, 45–56.

33 S. Chang, M. Wang, Y. Tian, J. Qi and Z. Qiu, *Chin. Med.*, 2020, **15**, 50.

34 P. C. Estabile, M. C. de Almeida, E. B. Campagnoli, M. A. Santo, M. R. da S. Rodrigues, F. Q. Milléo and R. F. Artoni, *Arq. Bras. Cir. Dig.*, 2022, **35**, e1651.

35 N. Vhora, U. Naskar, A. Hiray, A. S. Kate and A. Jain, *Rev Diabet Stud.*, 2020, **16**, 13–23.

36 F. S. Felix and L. Angnes, *Biosens. Bioelectron.*, 2018, **102**, 470–478.

37 F. Mollarasouli, S. Kurbanoglu and S. A. Ozkan, *Biosensors*, 2019, **9**(3), DOI: 10.3390/bios9030086.

38 A. A. Homaei, R. Sariri, F. Vianello and R. Stevanato, *J. Chem. Biol.*, 2013, **6**, 185–205.

39 P. Malik, R. Gupta, V. Malik and R. K. Ameta, *Measur. Sens.*, 2021, **16**, 100050.

40 M. M. Sabzehmeidani, S. Mahnaee, M. Ghaedi, H. Heidari and V. A. L. Roy, *Adv. Mater.*, 2021, **2**, 598–627.

41 S. E. Elugoke, O. E. Fayemi, A. S. Adekunle, B. B. Mamba, T. T. I. Nkambule and E. E. Ebenso, *FlatChem*, 2022, **33**, 100372.

42 S. Rizvi, S. Rouhi, S. Taniguchi, S. Y. Yang, M. Green, M. Keshtgar and A. Seifalian, *Int. J. Nanomed.*, 2014, **9**, 1323–1337.

43 X. Hu, Y. Li, Y. Xu, Z. Gan, X. Zou, J. Shi, X. Huang, Z. Li and Y. Li, *Food Chem.*, 2021, **339**, 127775.

44 B. K John, T. Abraham and B. Mathew, *J. Fluoresc.*, 2022, **32**, 1–23.

45 Y. Wang and A. Hu, *J. Mater. Chem. C*, 2014, **2**, 6921–6939.

46 M. He, J. Zhang, H. Wang, Y. Kong, Y. Xiao and W. Xu, *Nanoscale Res. Lett.*, 2018, **13**, 175.

47 R.-Z. Gong, Y.-H. Wang, Y.-F. Wang, B. Chen, K. Gao and Y.-S. Sun, *Molecules*, 2018, **23**(12), DOI: 10.3390/molecules23123316.

48 L. Kuang, Z. Jing, J. Wang, L. Ma, X. Liu and J. Yang, *J. Pharm. Biomed. Anal.*, 2014, **90**, 1–6.

49 R. Petrovič, J. Futas, J. Chandoga and V. Jakuš, *Biomed. Chromatogr.*, 2005, **19**, 649–654.

50 B. Ciui, M. Tertis, C. N. Feurdean, A. Ilea, R. Sandulescu, J. Wang and C. Cristea, *Sens. Actuators, B*, 2019, **281**, 399–407.